

Triple-Phase-Shift Controlled Dual Active Bridge Converter with Variable Input Voltage in Auxiliary Railway Supply

Martin Scohier, Olivier Deblecker, Carlos Valderrama
Electrical Engineering Division, Engineering Faculty, University of Mons
31, Bd. Dolez
Mons, Belgium
Phone: +3265374154
Email: martin.scohier@umons.ac.be
URL: <https://www.epeu-umons.be/>

Acknowledgments

The authors would like to thank C. Versèle, Alstom Belgium, for supporting this work.

Keywords

«Railway power supply», «On-board auxiliary power supply system», «Dual Active Bridge (DAB)», «DC-DC», «Simulation»

Abstract

Modern railway auxiliary supply uses a Dual-Active-Bridge whose input voltage, subject to variations, is regulated by means of a front-end boost stage. With the aim of gaining weight and simplicity, this paper proposes to implement Triple-Phase-Shift modulation in order to maintain high performance when this front-end stage is removed. Analytical models including a more accurate magnetic power losses calculation are developed and results in terms of efficiency are presented for comparison.

Introduction

Due to increased comfort and higher traveling speed demands, modern railways coaches require a continuous energy supply to auxiliary equipment such as air conditioning, lighting, pressure protection, etc. Due to the different voltage levels of the catenary across the world, the electric energy from the locomotive is transferred to the coaches via a supply line with the nominal voltage varying from 750 V to 3 kV in the case of a dc catenary [1]. The supply voltage of the consumers connected to such an electricity supply unit reaches from a few tenths of volts for battery charger to three-phase 400 V ac. The power level is typically within the range of few hundreds of kilowatts and a galvanic isolation is required for safety reasons.

Today, new auxiliary power supplies consist of a multiport isolated dc-dc converter to interface the dc input, the battery and the output dc-ac module (see Fig. 1). An input LC filter is used for harmonic rejection, supply line overvoltage mitigation, etc. Such a power supply is constrained by numerous design considerations. For instance, low volume and mass (i.e. a high power density), high efficiency and bidirectional power flow are required. To that end, in recent applications, a Multiple Active Bridge (MAB) converter has been adopted, with a front-end boost converter to adapt the supply line voltage, that is subject to wide variations (typically $\pm 33\%$ of the rated value for a 1.5 kV dc catenary [1]), to the desired (regulated) level. Note that, in this study, the battery port will not be considered in a first approach; hence, a Dual Active Bridge (DAB) converter [2],[3] is considered (instead of a MAB). The corresponding circuit diagram is shown in Fig. 2. The medium-frequency (MF) transformer provides the mandatory galvanic isolation between the high voltage side and the consumers.

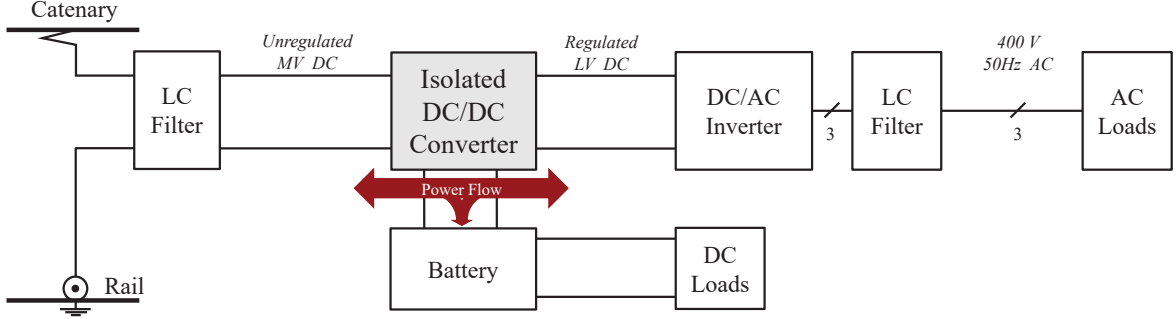


Fig. 1: Typical auxiliary power supply system with multiport isolated dc-dc converter

In this context, with a view of decreasing the mass and volume, the present paper aims to assess the feasibility of removing the 3-level boost converter shown in Fig. 2, hence simplifying the whole power conversion chain. The corresponding simplified topology of isolated dc-dc converter is shown in Fig. 3. This however leads to a nonregulated dc voltage at the input of the DAB, which makes the conventional Single Phase Shift (SPS) control strategy inappropriate for the considered application. Indeed, it is well established that despite the remarkable energy density of the DAB, most of its performance is highly dependent on the input/output voltage gain [2], [3],[4]. More concretely, poor efficiency and high current stress will occur as this gain departs from the MF transformer turns ratio. Therefore, in this contribution, it is proposed to adopt the Triple-Phase-Shift (TPS) modulation technique to overcome these limitations and extend the possibilities of the DAB converter. Several papers already addressed TPS controlled DAB converter operation focusing on various objectives (see, e.g., [2]-[6]). However, to our knowledge, addressing the application of a railway power supply with unregulated input voltage is a novelty.

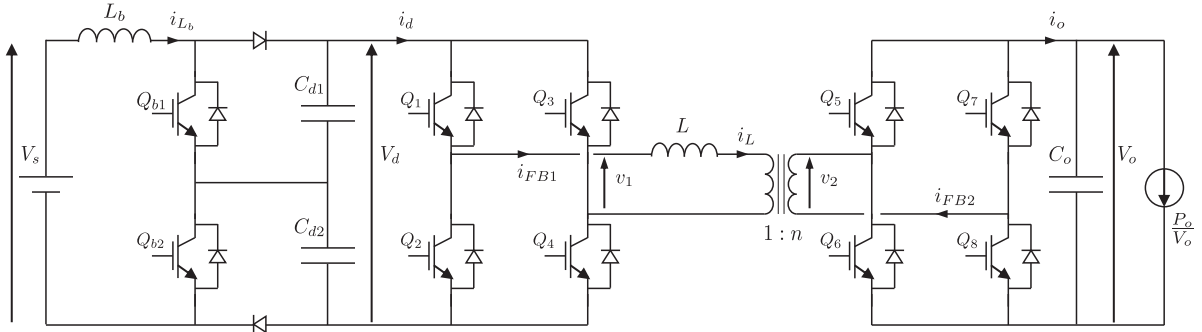


Fig. 2: Isolated dc-dc converter with front-end 3-level boost converter

Triple-Phase-Shift technique exploits the inner duty cycles of the primary- and secondary-side full bridge of the DAB converter (D_1 and D_2) in combination with the outer phase shift duty cycle D_3 in order to shape the inductor current i_L in the preferred way depending on the operating conditions. Fig. 4a shows some typical waveforms obtained with TPS by way of example. An overview of TPS modulation techniques can be found in [3], [4]. In this work, a backflow power minimization TPS strategy [7] is considered due to its effectiveness and because the modulation parameters (i.e. the duty ratios) can be quickly calculated using analytical formulae.

The remainder of this paper is organized as follows. The main assumptions and converter specifications (including the MF frequency transformers) are first presented. Then, analytical converter models are introduced followed by the main relationships used for power loss calculation. The results in terms of efficiency and power loss distribution obtained for the two isolated dc-dc converter solutions are presented in the next section. Finally, a discussion is being held to highlight the pros and cons of using TPS modulation strategy for the considered application.

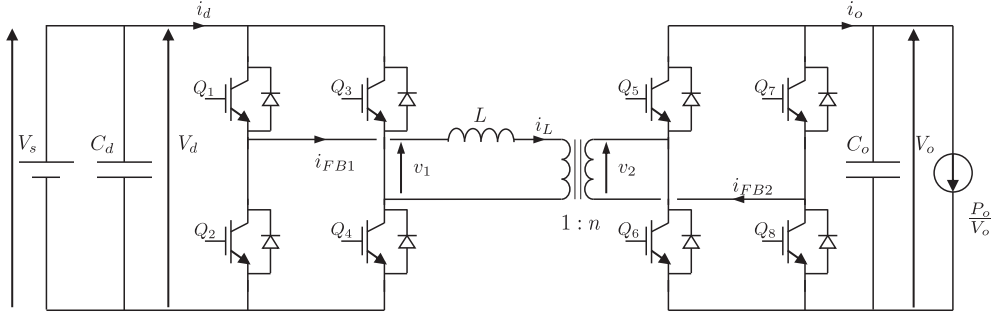


Fig. 3: Isolated dc-dc converter without front-end stage

Assumptions and specifications

Because output dc/ac module operation, filter design and battery management are not in the scope of this paper, assumptions are made to simplify the comparison between the two solutions of isolated dc-dc adaptation stage (namely with and without front-end boost converter) in steady-state. As already mentioned, the battery port is not considered. Moreover, it is initially assumed that the power flow is unidirectional from the dc voltage supply to a dc load (represented by a constant current source). The catenary voltage V_s is assumed constant within the permitted range. Input and output voltages of the DAB converter are considered as constant voltage sources assuming large capacitors.

Table I gives the main specifications and operating conditions used in this work. A 1.5 kV dc catenary voltage supply is chosen but it can vary from 1 kV to 2 kV [1]. In Fig. 2, the voltage V_d downstream of the 3-level boost converter is selected to be 2 kV, i.e. the upper limit of the supply line voltage. As IGBT modules are more mature at these voltage ratings and also due to data availability from manufacturer's datasheet, this technology is chosen here. Hence, the switching frequency f_s is set to 5 kHz.

Table I: Converter specifications

	Symbol	With boost converter	Without boost converter
Output Power Range	P_o	10 ~ 150 kW	10 ~ 150 kW
Supply dc voltage	V_s	1 ~ 2 kV	1 ~ 2 kV
DAB Input dc voltage	V_d	2 kV	1 ~ 2 kV
DAB Output dc voltage	V_o	750 V	750 V
Switching frequency	f_s	5 kHz	5 kHz

Transformer specifications

The absence of a front-end regulation circuit leads to a varying peak magnetic flux density in the core and increases rms currents in the windings. Since the MF transformer is one of the key elements of the converter, an accurate model is necessary for the comparison. First, the transformer turns ratio $n = V_o/V_d$ is set to match the DAB input and output voltage ratio under normal conditions (in this regard, V_d is equal to 2 kV or 1.5 kV according to whether the front-end boost stage is present or not). Applying a rule of thumb, the ac inductance L is determined with the SPS power transfer equation [2] ensuring that the maximum power is transferred with an outer phase shift D_3 of one eighth (i.e. 45 degrees) of the switching period. In that equation, the DAB input voltage V_d is selected to be 2 kV or 1 kV (i.e. the lower bound of the supply dc voltage), depending on whether the the boost stage is present or not). The area product design method allows to determine both electrical and geometrical characteristics of the transformer for each configuration. A ferrite double-E shaped core is adopted here for the sake of simplicity. Indeed, the optimal dimensions of such a common shape are easily derived from the so-called area product, i.e. the product of the core cross section area A_{core} and the winding window area A_{wind} (see (1)). Moreover, in an effort to reduce the ac resistance value, aluminium Litz wire is considered in the windings. The area

product can also be expressed as follows :

$$A_p = A_{core} \cdot A_{wind} = \frac{V_{1,rms}}{k_f f_s B_m} \frac{2I_{L,rms}}{J k_u} \quad (1)$$

where f_s , $V_{1,rms}$ and $I_{L,rms}$ depend on the converter specifications. The peak value of magnetic flux density B_m and the peak current density J are adjustable parameters. Because optimal design of the transformer is not in the scope of this project, such parameter values are derived from the works conducted in [8] for a similar power level and comparable converter specifications. Therefore, B_m is set to 0.15 T and J is taken equal to 3 A/mm². The form factor k_f is equal to 4 in the case of triangular shaped magnetic flux density. The utilization factor k_u of a Litz wiring is typically equal to 0.3. Furthermore, the transformer is assumed to be designed in a way to match its total leakage inductance with the desired ac link inductance L . As for the magnetizing inductance, based on previous railway auxiliary power supply projects, its value is fixed to limit the peak amplitude of the magnetizing current under 10% of the primary side maximum rms current ($L_m = V_{1,rms} / (k_f f_s \cdot 0.1 \cdot I_{L,rms})$). The mass of the transformer m_{TFO} is calculated from the core and winding volume along with their respective material mass densities. Hence, Table II shows the specifications adopted for the MF transformer in both isolated dc-dc converters.

Table II: Transformer specifications

	Symbol	With boost converter	Without boost converter
Transformer Turns Ratio	n	3/8	1/2
Primary side maximum rms Voltage	$V_{1,rms}$	2 kV	2 kV
Primary side maximum rms Current	$I_{L,rms}$	91 A	167 A
Core cross section	A_{core}	120 cm ²	163 cm ²
Core volume	V_{core}	10 dm ³	15 dm ³
Total dc resistance	R_{dc}	116 mΩ	55 mΩ
Total leakage inductance	$L = l_1 + l_2'$	500 μH	187.5 μH
Magnetizing inductance	L_m	10.9 mH	6 mH
Mass of the transformer	m_{TFO}	70 kg	111 kg

Modeling of the converter operation

In order to obtain the key waveforms of the two isolated dc-dc adaptation stages, analytical converter models valid under steady-state operation are implemented. The first model concerns the DAB converter when used with TPS modulation (noticing that SPS modulation is a specific case of TPS in which $D_1 = D_2 = 1$). It includes an accurate operation of the MF transformer. The second model relates to the 3-level boost converter possibly connected at the input of the DAB converter.

A lossless operation of the converter is assumed to obtain the current waveforms in each power switch and passive component. For each configuration of the dc-dc adaptation stage, the output power and input voltage are swept within their respective ranges of values. The duty cycles D_1 , D_2 and D_3 are calculated according to the chosen modulation strategy. The voltages at the ports of the MF transformer can be defined as $v_1(t) = V_d \cdot s_1(t)$ and $v_2'(t) = V_o/n \cdot s_2(t)$, where s_1 and s_2 are the switching functions of the DAB primary and secondary side (see (2)). The inductor current is governed by (3) considering the simplified ac link circuit in Fig. 5a. The characteristic waveforms of the inductor current and the switch gate drive signals are shown in Fig. 4a. Here, the switching cycle starts when the power switch Q_1 turns on ($t_{2 \rightarrow 1} = 0$). Hence, considering TPS modulation, the switching instants are defined as follows over the first half of the switching period : $t_{4 \rightarrow 3} = D_1 T_s / 2$, $t_{6 \rightarrow 5} = D_3 T_s / 2$ and $t_{8 \rightarrow 7} = (D_3 + D_2) T_s / 2$.

$$s_1(t) = \begin{cases} 1, & 0 < t < D_1 \frac{T_s}{2} \\ 0, & D_1 \frac{T_s}{2} < t < \frac{T_s}{2} \\ -1, & \frac{T_s}{2} < t < (1+D_1) \frac{T_s}{2} \\ 0, & (1+D_1) \frac{T_s}{2} < t < T_s \end{cases} \quad s_2(t) = \begin{cases} 1, & D_3 \frac{T_s}{2} < t < (D_3 + D_2) \frac{T_s}{2} \\ 0, & (D_3 + D_2) \frac{T_s}{2} < t < (1+D_3) \frac{T_s}{2} \\ -1, & (1+D_3) \frac{T_s}{2} < t < (1+D_3 + D_2) \frac{T_s}{2} \\ 0, & (1+D_3 + D_2) \frac{T_s}{2} < t < D_3 \frac{T_s}{2} + T_s \end{cases} \quad (2)$$

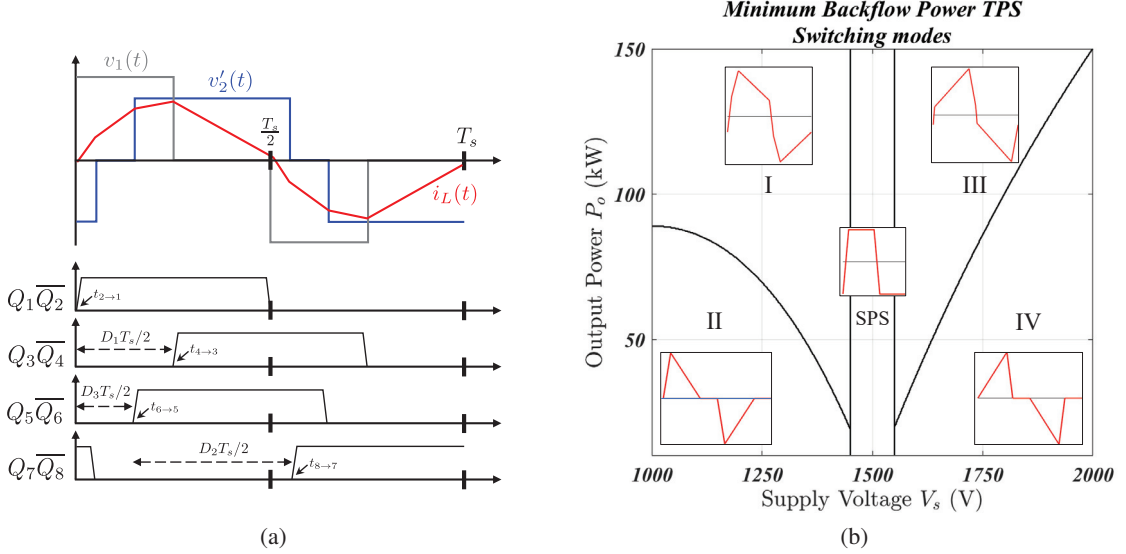


Fig. 4: (a) Characteristic waveforms using TPS modulation. (b) Minimum backflow power TPS strategy : existing modes and their inductor current typical waveform

$$L \frac{d i_L(t)}{dt} = v_1(t) - v'_2(t) \quad (3)$$

The proposed TPS modulation strategy, aiming to minimize the reactive power in the ac link, switches between five modes depending on the output power and the ratio between input and output voltage of the DAB converter [7] (see Fig. 4b). First, SPS modulation is applied when the voltage is near its nominal value, i.e. when $V_s = 1500 \pm 50$ V. Then, if the input voltage deviates from this range, the current is shaped into a discontinuous triangular waveform for light load conditions (modes II & IV). The other two modes (I & III) involve the calculation of optimal duty cycle values and are employed at higher power levels.

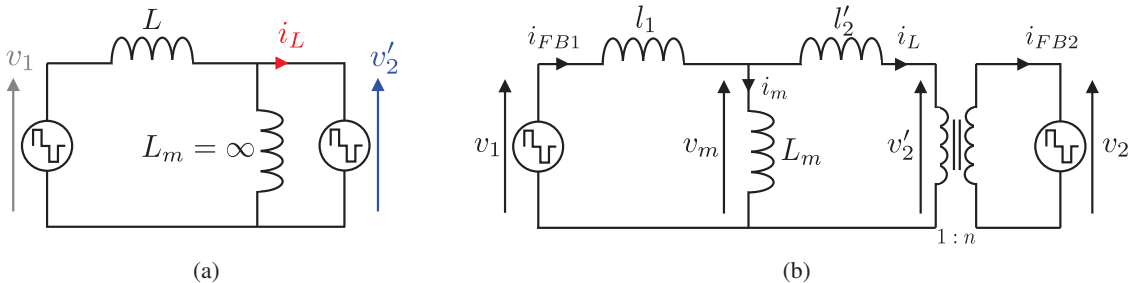


Fig. 5: (a) Lossless ac link circuit ($i_m = 0$). (b) Lossless ac link circuit ($i_m \neq 0$)

In this contribution, in an attempt to better describe the operation of the transformer, the magnetizing current is considered resulting in a more accurate model of the ac link (see Fig. 5b). The analytical expression of the voltage v_m across the magnetizing inductance L_m is given by (4), assuming an equal distribution of the leakage inductances and a large magnetizing inductance.

$$v_m(t) = \frac{v_1(t)l'_2 + v'_2(t)l_1}{(l_1 + l'_2 + \frac{l_1l'_2}{L_m})} \approx \frac{v_1(t) + v'_2(t)}{2} \quad (4)$$

The magnetizing current is governed by :

$$L_m \frac{d i_m(t)}{dt} = v_m(t) \quad (5)$$

Then, the ac currents of both full bridges, namely i_{FB1} and i_{FB2} , are determined assuming that the primary side full bridge (FB1) conducts the magnetizing current. Therefore, $i_{FB1}(t) = i_L(t) + i_m(t)$ and $i_{FB2}(t) = i_L(t)/n$. Depending on the direction of these currents and with the use of the switching functions in (2), the current waveforms can be obtained for each semiconductor device (transistor or anti-parallel diode).

In the front-end boost stage, whose operation is exposed in [9], the duty cycle depends on the input and output voltage ($D_b = 1 - V_s/V_d$). Similarly to the DAB, a switching function can be determined to reflect the state of the converter. Moreover, the current waveforms in each device are derived from the boost inductor current i_{L_b} . The average value is equal to P_o/V_s and the peak-to-peak current ripple is given by

$$\Delta I_{L_b} = \left(V_s - \frac{V_d}{2} \right) \frac{D_b}{f_s L_b} \quad (6)$$

Power loss calculation

Due to the skin effect, the resistance of the Litz wire at the fundamental frequency of 5 kHz is assumed to be 1.5 times larger than the dc resistance [10]. Therefore, winding losses in the transformer can be calculated by means of $P_{TFO,wind} = 1.5R_{dc}I_{FB1,rms}^2$ where R_{dc} is the total dc resistance of the windings viewed from the primary side and $I_{FB1,rms}$ is the rms value of the ac current of FB1.

Magnetic power losses are usually evaluated with the Improved Generalized Steinmetz Equation (IGSE) because of its accuracy for non-sinusoidal induction [11]. Contrary to most existing works, this paper proposes to consider the exact time evolution of the magnetic flux density according to the governing equation (7), where N_1 is the number of turns of the transformer primary winding. The volume and the cross section area of the ferrite core are denoted V_{core} and A_{core} , respectively. Moreover, the steinmetz coefficients in (8) are selected from [11] and have the following values : $\alpha = 1.25$, $\beta = 2.35$ and $k = 16.9$.

$$\frac{dB(t)}{dt} = \frac{v_m(t)}{A_{core}N_1} \quad (7)$$

$$P_{TFO,core} = V_{core} \left(\frac{\Delta B}{2} \right)^{\beta-\alpha} \frac{k_i}{T_s} \int_0^{T_s} \left| \frac{dB}{dt} \right|^{\alpha} dt \quad \text{with} \quad k_i = \frac{k}{(2\pi)^{\alpha-1} \int_0^{2\pi} |\cos \theta|^{\alpha} d\theta} \quad (8)$$

The current and voltage waveforms calculated from the analytical converter models are used to select the IGBT modules. Their ratings are listed in Table III. The conduction losses of the devices (diodes and IGBTs) are calculated from their average and rms currents (denoted I_{avg} and I_{rms} , respectively) given the well-known formula

$$P_{cond} = V_{th}I_{avg} + rI_{rms}^2 \quad (9)$$

where V_{th} represents the threshold voltage and r the on-state resistance taken from the manufacturers datasheets.

Table III: IGBT module

	Voltage rating V_{CE}	Current rating I_{CE}
3-level Boost	1.7 kV	150 A
DAB Full Bridge 1	3.3 kV	200 A
DAB Full Bridge 2	1.7 kV	200 A

Due to the large number of switching devices, switching losses tend to decrease the power density of the DAB converter. Soft switching is thus desired within the entire range of operation. As the use of parallel snubber capacitors is commonly adopted to lower the turn off losses, these will not be considered. However, due to the presence of snubber capacitors, the voltage across each switch will decrease slowly, resulting in losses at turn on [12], [13]. To prevent this, the capacitor must fully discharge during the dead-time between the switch gate signals in each leg, allowing the anti-parallel diode to conduct and

resulting in a quasi zero voltage turn on. This can be achieved if the dead-time is long enough and if the energy stored in the ac link inductance is sufficient. Moreover, it is generally adopted to simplify the ZVS turn-on condition to the sign of the inductor current at switching instants [4], [6]. Therefore, only hard switching loss at non-ZVS turn on is considered. For instance, equation (10) gives the average switching losses of the IGBT Q_1 over one switching period. The energy loss at turn on and turn off (E_{on} and E_{off}) are obtained from IGBT modules characteristics.

$$P_{swQ1} = \begin{cases} f_s E_{on}[i_{FB1}(t_{2 \rightarrow 1})], & \text{if } i_L(t_{2 \rightarrow 1}) < 0 \\ 0, & \text{if } i_L(t_{2 \rightarrow 1}) \geq 0 \end{cases} \quad (10)$$

The power switches in the 3-level boost converter operate in hard switching. Considering IGBT Q_{b1} as an example, the switching losses are calculated by using the following expression:

$$P_{swQb1} = f_s (E_{on}[i_{L_b}(t_{b2 \rightarrow b1})] + E_{off}[i_{L_b}(t_{b1 \rightarrow b2})]) \quad (11)$$

Finally, efficiency for each operating point of the converter within the admitted range is calculated using (12). $\sum P_{loss}$ stands for the total of losses including $P_{TFO,core}$, $P_{TFO,wind}$, $P_{DAB,cond}$, $P_{DAB,sw}$, $P_{Boost,cond}$ and $P_{Boost,sw}$.

$$\eta = \frac{P_o}{P_o + \sum P_{loss}} \quad (12)$$

Results

In this section, the simulations based on the above analytical models are conducted assuming three different cases. The first one (denoted as SPS case) concerns the DAB converter using SPS modulation directly connected to the varying voltage supply (as in Fig. 3) and exposes the limitations when the DAB converter faces varying operating conditions. The two other cases (simply denoted here as BOOST and TPS cases) address these limitations by using two different approaches which is the subject of a comparison. In the so-called BOOST case, a DAB converter with SPS modulation is used in combination with a front-end three-level boost stage (see the dc-dc converter configuration shown in Fig. 2). In the TPS case, the disadvantage of the non-regulated voltage at the input of the DAB converter is compensated by switching between modulation modes depending on the operating conditions. The isolated dc-dc converter operation over a switching period is simulated for a set of operating points, defined by values of the catenary voltage V_s and the output power P_o (within the ranges specified in Table I). Hence, the power losses can be calculated by exploiting the computed voltage and current waveforms at each operating point. In this way, Fig. 6 shows the ensuing efficiency maps for the three different cases considered here. Furthermore, Fig. 7 shows the efficiency curves under minimum, rated and maximum supply voltage conditions.

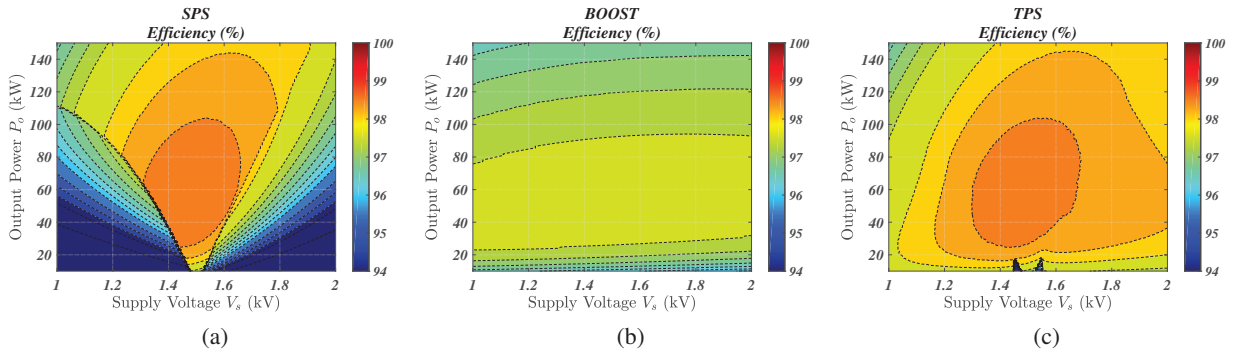


Fig. 6: Efficiency maps of the isolated dc-dc converter in the SPS, BOOST and TPS cases

It is first to be noted that the DAB converter with SPS modulation is subject to large power losses when

the input voltage deviates from the nominal value (see Fig. 6a). This is even more pronounced in the case of light load conditions, given the high reactive power circulating in the circuit. Additionally, hard switching losses occur as the direction of the ac currents are no longer favorable for ZVS turn on. In Fig. 6b, the advantage of an input voltage regulation is exposed. The BOOST case is advantageous because the efficiency remains nearly unchanged (about 97%), whatever the operating point taken within the limits of variation of the output power and supply voltage. It can be observed in Fig. 6c that TPS case decreases the power losses in the critical areas of the SPS case while maintaining an overall higher efficiency than in the BOOST case. These high efficiency values represent an upper bound due to the approached calculation (based on analytical formulae) and because other losses exist in the converter (non-zero soft switching losses, losses in the filtering elements, etc.). At rated dc voltage supply, i.e. $V_s = 1.5$ kV, the DAB converter with no front-end boost stage is clearly advantageous in terms of efficiency (see Fig. 7b). This is due to the remarkable performances of SPS modulation when the input and output dc voltage ratio matches the transformer turns ratio.

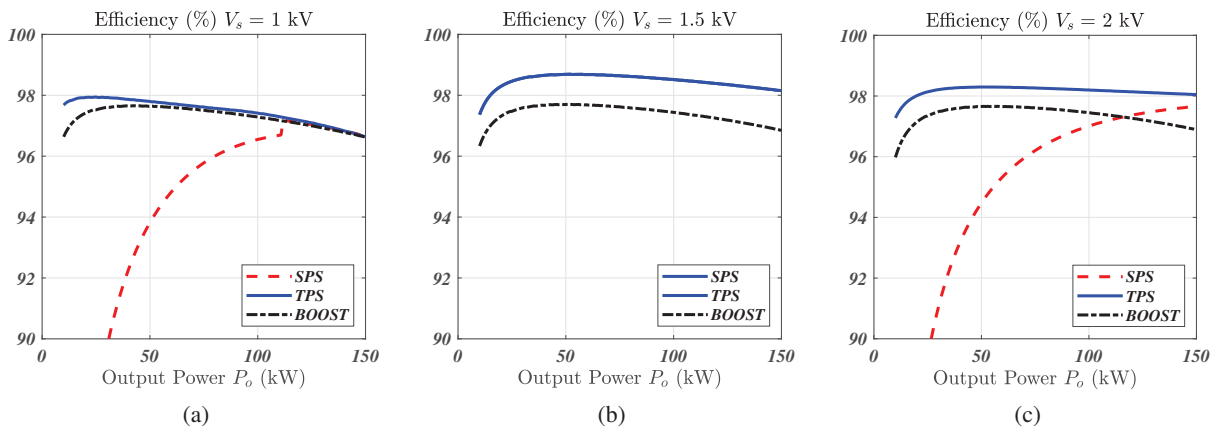


Fig. 7: Efficiency curves under different supply voltage conditions : (a) $V_s = 1$ kV, (b) $V_s = 1.5$ kV and (c) $V_s = 2$ kV

Fig. 8 shows the power loss distribution in the different components of the isolated dc-dc converter cases under different supply voltage ($V_s = 1$ kV, 1.5 kV and 2 kV), at rated and light load conditions (i.e. $P_o = 150$ kW and 50kW, respectively). The DAB converter power losses mainly consist of conduction losses in the IGBT modules and in the transformer windings. Switching losses predominate in the three-level boost converter as only hard-switching occurs. On the other hand, soft switching is achieved in the DAB converter for the whole range of operation for the two compared dc-dc adaptation stage solution (see BOOST and TPS cases). As it can be observed in Fig. 8a and Fig. 8c, the TPS modulation in modes I and III (i.e. the modes that are used at high power level) shows slight improvement with regard to the SPS modulation.

Magnetic power losses in the ferrite core are relatively small due to the low switching frequency. Yet, they form a more important part of the transformer total losses when the load decreases. Due to their dependency on the DAB primary and secondary side voltage levels, such power losses tend to vary widely when the input voltage of the DAB is no longer regulated. Nevertheless, because of its ability to tune both inner duty cycles, applying TPS modulation strategy allows to reduce the peak magnetic flux density in the core resulting in fewer magnetic power losses than in the two other cases studied (SPS and BOOST).

The current waveforms in the filter capacitors can be computed as well from the analytical converter models. Considering the fundamental harmonic only ($=2f_s$), the removal of the front-end stage leads to an increase of the maximum rms value from 88 A to 167 A in the output filter capacitor C_o (for the BOOST and TPS cases, respectively). Therefore, a higher capacitance value (about twice as large) must be chosen in order to keep a comparable output voltage ripple. The same calculation for the input filter capacitor gives no variation regarding the maximum rms value of the current. However, the comparison

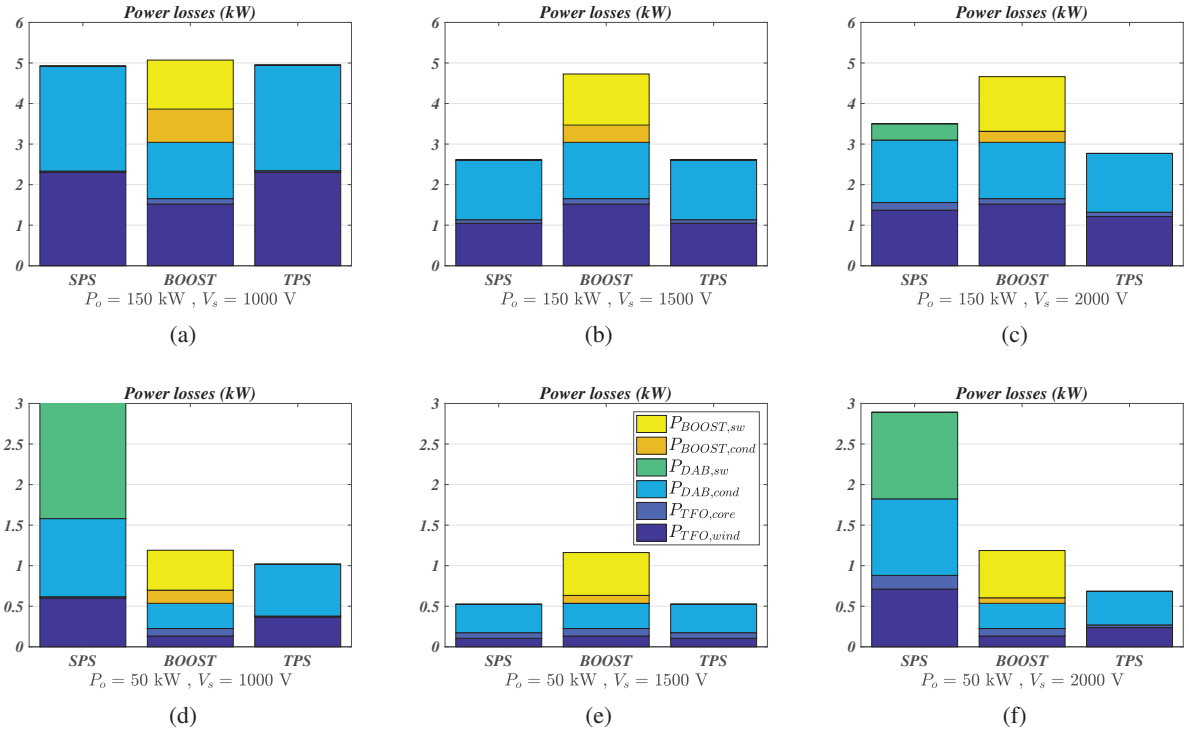


Fig. 8: Power loss distribution

analysis is not as straightforward as their role and topology in the two isolated dc-dc converter solutions are very different (see Fig. 2 and Fig. 3).

Discussion

As observed in previous section, for the considered specifications, the proposed isolated dc-dc converter with no front-end boost stage shows high performance at nominal voltage due to the optimal utilization of the SPS modulation and the elimination of the losses in the front-end stage. Moreover, the TPS modulation greatly improves the efficiency of the converter in case of severe voltage conditions. This is mainly due to the triangular shaped current which maintains minimal switching losses while decreasing the rms value of the ac link current at light load. Nevertheless, these results should be experimentally validated in future work.

From a component point of view, it is straightforward that removing the front-end stage will reduce the number of parts, in particular the front-end boost stage components. However, input voltage variation of the DAB converter will accordingly lead to higher thermal constraints and increased stresses on the remaining components, leaving the gain in terms of mass and volume uncertain. A higher capacitance value and rms currents in the output filter leads to a larger capacitor. Regarding the primary- and secondary-side full bridge of the DAB converter, while IGBT modules ratings are suitable for both configurations of isolated dc-dc converter, overall higher conduction losses as depicted in Fig. 8 will lead to the design of bulkier and heavier heatsinks. Furthermore, due to increased current at low supply voltage, the design method has resulted in a bigger and heavier transformer solution. The higher mass of the proposed MF transformer is compensated by lower losses and a wider cooling area, resulting in lower thermal management constraints. In a will to increase the power density, higher switching frequencies in combination with MOSFET SiC technologies will be increasingly used [3]. This will reduce the size of the passive elements as well as the overall power losses in the switches. In this context, the magnetic losses will become a more significant consideration, hence making the use of TPS modulation more relevant in such applications.

Finally, TPS modulation involves two extra degrees of freedom (D_1 and D_2) compared to SPS modulation

strategy. It is therefore more difficult to implement in practice. Additionally, depending on the operating point, five different modes of operation exist which need to be switched accordingly from one to another (see Fig. 4b). Note that in this application, at high power level, the possibility of ignoring modes I and III to gain simplicity could be explored. On the other hand, the voltage controller (with inner current loop) necessary to regulate the output voltage of the 3-level boost stage is no longer necessary if the simplified configuration of isolated dc-dc converter is adopted, which is an asset.

Conclusion

This paper focused on a modern auxiliary power supply with bidirectional power flow capability. An isolated dc-dc converter is used to provide a (regulated) dc voltage at the input of the dc/ac module. Leaving apart the battery port, the topology of this converter is currently composed of a front-end 3-level boost stage and a DAB converter operated via SPS modulation strategy. The possibility of removing the front-end stage has been investigated by means of steady-state simulations conducted using analytical models, within the whole range of operation points in terms of output power and catenary supply voltage. In an effort to better compare the two dc-dc converter solutions, an analytical model of the MF transformer losses taking into account the magnetizing current has been employed. Based on simulation results, it was shown that using a minimum reactive power TPS strategy increases the overall efficiency of the isolated dc-dc converter. However, increased stresses is responsible for bulkier elements when removing the front-end circuit, with particular regard to the MF transformer. Moreover, it can be expected to simplify the control structure.

References

- [1] BS EN 50163 Railway applications. Supply voltages of traction systems
- [2] Krismer, Florian. "Modeling and optimization of bidirectional dual active bridge DC-DC converter topologies." (2010).
- [3] B. Zhao, Q. Song, W. Liu and Y. Sun, "Overview of Dual-Active-Bridge Isolated Bidirectional DC-DC Converter for High-Frequency-Link Power-Conversion System," in IEEE Transactions on Power Electronics, vol. 29, no. 8, pp. 4091-4106, Aug. 2014, doi: 10.1109/TPEL.2013.2289913.
- [4] N. Hou and Y. W. Li, "Overview and Comparison of Modulation and Control Strategies for a Nonresonant Single-Phase Dual-Active-Bridge DC-DC Converter," in IEEE Transactions on Power Electronics, vol. 35, no. 3, pp. 3148-3172, March 2020, doi: 10.1109/TPEL.2019.2927930.
- [5] J. Huang, Y. Wang, Z. Li and W. Lei, "Unified Triple-Phase-Shift Control to Minimize Current Stress and Achieve Full Soft-Switching of Isolated Bidirectional DC-DC Converter," in IEEE Transactions on Industrial Electronics, vol. 63, no. 7, pp. 4169-4179, July 2016, doi: 10.1109/TIE.2016.2543182.
- [6] Y. Tang et al., "RL-ANN Based Minimum-Current-Stress Scheme for the Dual Active Bridge Converter with Triple-Phase-Shift Control," in IEEE Journal of Emerging and Selected Topics in Power Electronics, doi: 10.1109/JESTPE.2021.3071724.
- [7] S. Shao, M. Jiang, W. Ye, Y. Li, J. Zhang and K. Sheng, "Optimal Phase-Shift Control to Minimize Reactive Power for a Dual Active Bridge DC-DC Converter," in IEEE Transactions on Power Electronics, vol. 34, no. 10, pp. 10193-10205, Oct. 2019, doi: 10.1109/TPEL.2018.2890292.
- [8] C. Versele, O. Deblecker and J. Lobry, "Multiobjective optimal design of high frequency transformers using genetic algorithm," 2009 13th European Conference on Power Electronics and Applications, 2009, pp. 1-10.
- [9] M. T. Zhang, Yimin Jiang, F. C. Lee and M. M. Jovanovic, "Single-phase three-level boost power factor correction converter," Proceedings of 1995 IEEE Applied Power Electronics Conference and Exposition - APEC'95, 1995, pp. 434-439 vol.1, doi: 10.1109/APEC.1995.468984.
- [10] Mohan, Ned, Tore M. Undeland, and William P. Robbins. Power electronics: converters, applications, and design. John wiley & sons, 2003.
- [11] Hurley, William G., and Werner H. Wölflé. Transformers and inductors for power electronics: theory, design and applications. John Wiley & Sons, 2013.
- [12] Naayagi, R., & Mastorakis, N. (2012). Performance verification of dual active bridge DC-DC converter. ACA'12 Proceedings of the 11th International Conference on Applications of Electrical and Computer Engineering, 1(October), 13–19.
- [13] Sommer, F., Menger, N., Merz, T., & Hiller, M. (2021). Accurate Time Domain Zero Voltage Switching Analysis of a Dual Active Bridge with Triple Phase Shift. 2021 23rd European Conference on Power Electronics and Applications, EPE 2021 ECCE Europe, 1–9.